Magnetic structure and spin dynamics of the Pr and Cu in Pr_2CuO_4

I. W. Sumarlin and J. W. Lynn
Center for Superconductivity Research, Department of Physics, University of Maryland, College Park, Maryland 20742 and Reactor Radiation Division, National Institute of Standards and Technology, Gaithersburg, Maryland 20899

T. Chattopadhyay
Institut Laue-Langevin Boîte Postale 156X, 38042 Grenoble Cedex, France

S. N. Barilo and D. I. Zhigunov
Institute of Physics of Solids and Semiconductors, Belarus Academy of Sciences, 220726 Minsk, Belarus

J. L. Peng
Center for Superconductivity Research, Department of Physics, University of Maryland, College Park, Maryland 20742
(Received 5 October 1994)

Neutron-scattering techniques have been used to study the magnetic structure and spin dynamics of the Pr and Cu spins in Pr_2CuO_4. In the ordered state the Cu spin-wave velocity c has been determined to be 0.85 ± 0.08 eV Å, which corresponds to an in-plane nearest-neighbor exchange constant $J=130\pm13$ meV. A spin-wave gap of ~5 meV has been observed, corresponding to a reduced anisotropy constant $\alpha_{\|}=(J-J^{xy})/J$ of $\sim2\times10^{-4}$. In the paramagnetic regime the evolution of the Cu spin-correlation length with temperature is adequately described by the renormalized classical theory for the quantum nonlinear sigma model. For the Pr ions, significant dispersion is observed for the first excited-state crystal-field level, directly demonstrating that there are Pr-Pr exchange interactions both within the a-b plane as well as along the c axis. These interactions along the c axis must be mediated through the CuO planes which are also involved in superconductivity in these cuprate materials. A singlet-doublet magnetic exciton model, with Pr-Pr Heisenberg exchange terms as large as ~0.8 meV, provides a good quantitative description of the measured dispersion relations. The temperature dependence of the magnetic excitons also can be qualitatively understood with this theory if the exchange terms are modified by a temperature-dependent renormalization factor. The zero-field ordered moment at low temperatures for the Cu is determined to be $0.40\pm0.02\mu_B$, in good agreement with results reported by other groups. However, field-dependent diffraction measurements suggest that the correct Cu spin structure is the noncollinear one, where spins in adjacent layers along the c axis are orthogonal, rather than the collinear structure assumed by other groups. This noncollinearity is also reflected in the configuration of the small induced moments ($0.08\pm0.005\mu_B$) that develop at low temperatures on the Pr ions. The magnetic-field–temperature phase diagram for the case of an applied field along the $[1\bar{1}0]$ direction reveals that the spin-rotation energy increases rapidly with decreasing temperature from ~200 K down to 4.5 K.

I. INTRODUCTION

Magnetism studies of the insulating R_2CuO_4 materials and their electron-doped superconducting compounds $R_{2-x}Ce_xCuO_4$ (R =Pr, Nd, Sm, and Eu) have shown that these materials exhibit a variety of interesting magnetic behavior involving both the rare-earth and the copper spins.[1–14] The very strong Cu-O bonding in the a-b plane gives rise to a magnetic energy scale much larger than the typical phonon energy scale, and produces two-dimensional- (2D) like magnetic behavior;[4,14] the weak exchange coupling along the c axis then induces long-range antiferromagnetic order at a relatively modest T_N in the range 250–300 K.[2–12] Hence the Cu spins provide one of the best physical realizations of a 2D quantum Heisenberg antiferromagnet—a system of central importance itself in the study of quantum magnets.[15–18] No long-range order is observed in the superconducting phase, but the large magnetic energy scale within the Cu-O planes persists, and has supported speculation that magnetism may be directly involved in the formation of the superconducting state. The rare-earth ions, on the other hand, typically order at much lower temperatures (≤6 K) in both the insulating and the superconducting phases.[9–13] The coexistence of long-range rare-earth magnetic order with superconductivity in these systems has provided an interesting situation where the interplay between the two cooperative phenomena can be studied.

In this paper, we report our neutron-scattering studies of the magnetic structure and spin dynamics of the Pr and Cu spins in Pr_2CuO_4, which address three aspects concerning the magnetism of this class of materials. The first aspect concerns the dynamics of the Cu spins, which are dominated by the huge isotropic in-plane exchange interactions. The spin-wave branches propagating in the a-b plane are thus highly dispersive, but we have been

0163-1829/95/51(9)/5824(16)/$06.00

able to resolve the $+q$ and the $-q$ branches of these modes, and thereby make a direct determination of the spin-wave velocity and corresponding isotropic in-plane exchange constant. Moreover, no significant dispersion of the spin-wave excitations was observed for propagation along the c axis, which reflects the underlying 2D nature of the magnetic interactions. The 2D in-plane correlations between the Cu spins persist at temperatures well above T_N, and the evolution of the 2D correlation length above T_N is well described by predictions[15,16] based on the renormalized classical theory of the 2D quantum nonlinear σ model, in analogy with the work done on similar systems.

The second aspect concerns the magnetism of the Pr ions. Previous inelastic-neutron-scattering measurements have demonstrated that Pr magnetic excitations predominantly are of the single-ion type in the form of transitions between crystal-field split levels of the ground-state multiplet, with an overall energy scale of ~ 88 meV.[19–23] In this scheme, the ground state is a nonmagnetic singlet, with the first excited state a doublet at ~ 18 meV. However, the net exchange field from the ordered Cu spins along with admixtures from higher state multiplets leads to an induced moment at low temperatures of $\sim 0.08\mu_B$ on the Pr,[4] which is much smaller than the free-ion value $gJ = 3.2\mu_B$. We measured this 18-meV singlet-doublet crystal-field transition and found that it exhibits dispersion as large as 1.2 meV, directly demonstrating significant exchange interactions between the Pr ions.[24] Moreover, this dispersion is observed for excitations propagating not only in the a-b plane, but along the c axis as well. The presence of magnetic interactions mediated through the copper-oxygen layers is significant in light of the fact that the same layers are involved in superconductivity in the electron-doped compounds. The measured data can be described quantitatively by a singlet-doublet magnetic exciton model analogous to that employed to describe Pr metal.[25–27] Our dynamical measurements of the Pr magnetic excitons are the first such studies of any rare-earth spins in the cuprate systems.

The final aspect of magnetism concerns the magnetic structure and the magnetic-field–temperature (H-T) phase diagram in the case of an applied field along the crystallographic $[1\bar{1}0]$ axis. Zero-field neutron-diffraction data cannot distinguish between the two proposed antiferromagnetic models for the Cu spin structures, namely, the collinear and the noncollinear model. The collinear model consists of spins that are either parallel or antiparallel along a single direction, the [110] direction in this case. The noncollinear model also consists of a simple antiferromagnetic arrangement of spins within each layer, with the spins along an edge direction, but an orthogonal arrangement between spins in adjacent layers. Thus the spin direction shifts from [100] to [010] from layer to layer. Resolving the ambiguity of the spin structure can be done via application of a symmetry-breaking magnetic field, and our field-dependent measurements with an applied field along $[1\bar{1}0]$ strongly suggests that the Cu spin structure is of the noncollinear type. This noncollinearity is also reflected in the configuration of the induced moments of the Pr ions. The same applied field was also used to measure the H-T phase diagram, which reveals a rapid increase of the spin-rotation energy with decreasing temperatures from ~ 200 K down to 4.5 K.

II. EXPERIMENTAL PROCEDURES

Pr_2CuO_4 crystallizes in the tetragonal T' structure (space group $I4/mmm$). The Cu ions occupy a body-centered tetragonal lattice, and in the a-b plane there are intervening O ions that form strong bonds, while there are no apical O ions in contrast to the La_2CuO_4 type materials. Hence the Cu-O sheets form a square-planar lattice. The Pr sublattice is of the same symmetry as the Cu but with a two-ion basis. We employed two single crystals in the present studies. One crystal weighed ~ 175 mg with approximate dimensions $1.5\times 1.2\times 0.05$ cm^3, and was used to investigate the magnetic Bragg intensities as a function of temperature and applied magnetic field. The room-temperature lattice constants are $a = 3.943$ Å and $c = 12.15$ Å and the observed Néel temperature of the Cu spins is 284 ± 1 K. The growth and preparation techniques can be found in the literature.[28] Zero-field data were collected at the BT-2 and BT-9 triple-axis spectrometers at the National Institute of Standards and Technology Research Reactor employing neutrons with energy 14.8 meV ($\lambda = 2.35$ Å), while the field-dependent data were collected at the NG-5 SPINS spectrometer using neutrons with energy 4.6 meV ($\lambda = 4.2$ Å). The (002) reflection of pyrolytic graphite (PG) crystals was used to monochromate the incident neutron beam.

The second sample was a much larger single crystal weighing ~ 7 g with approximate dimensions $2.8\times 2.2\times 0.2$ cm^3, and was used for our inelastic-neutron-scattering measurements of the spin dynamics. This crystal has lattice parameters of $a = 3.958$ Å and $c = 12.19$ Å at $T = 10$ K, and a Néel temperature of 251 ± 1 K. We note that both the lattice constants and Néel temperature are functions of the oxygen content.[29,30] Dynamical measurements were conducted at the BT-2 and BT-4 triple-axis instruments and the configuration was mostly in an energy-loss mode employing either fixed incoming or fixed final energy, with the use of a PG analyzer. The fixed neutron energies were typically 13.7 or 14.8 meV, while limited data were also obtained with fixed incident energies of 34.5 and 41 meV to crosscheck our results. Measurements of the Cu spin waves were made with the constant-energy method, whereas measurements of the Pr crystal-field excitations were made with the constant-**Q** technique. For measurements involving energy transfers ≥ 30 meV we used a Cu(220) monochromator which provides better resolution for these higher-energy transfers. Finally, for the measurements of the two-dimensional correlation length we used a PG(002) monochromator set to reflect neutrons with energy of 28 meV. No analyzer was used for these particular experiments to facilitate an experimental integration over energy. In all of our elastic and inelastic experiments, PG or cold Be filters were used to reduce contamination from higher-order wavelength neutrons below observable levels. Further instrumental details will

be given when the data are presented.

For the sample environment, we used closed-cycle helium displex refrigerators which have a temperature range from 10 to 500 K for the majority of the experiments. The sample was mounted for scattering experiments in the (hhl) scattering plane, and was sealed in an Al holder with helium-exchange gas, which was attached to the cold finger. A top-loading ILL-type cryostat that had a low-temperature capability of ~ 1.5 K was used for a few low-temperature measurements. Finally, for our field-dependent experiments we employed a vertical-field superconducting magnet capable of providing a maximum field of 7 T. The magnet is equipped with a dedicated helium-gas-flow cryostat capable of reaching liquid-helium temperatures.

III. FIELD-DEPENDENT DIFFRACTION MEASUREMENTS

A. Noncollinear spin structure

Below the (measured) $T_N = 284 \pm 1$ K a series of 3D magnetic Bragg peaks arising from the Cu spin ordering was observed in our zero-field diffraction experiments on the small crystal. All of the observed magnetic peaks can be indexed based on the chemical unit cell by the indices $(h/2, k/2, l)$, where h, k are odd integers and l is any integer. The same indexing is also found in all the other tetragonal R_2CuO_4 compounds.[2-7,12] The positions and intensities of these magnetic Bragg peaks can be accounted for quantitatively by *two* separate but related models for the Cu spin structure.[3-7,12] One possibility is the collinear model, in which spins are either aligned parallel or antiparallel to a single direction, as shown in Fig. 1(a). For Pr_2CuO_4 this direction must be the [110] in order to account for the observed intensities. The magnetic configuration can be described by an antiferromagnetic propagation vector $\mathbf{q}$ which is parallel to the ordered spins, and the magnetic symmetry is orthorhombic. There is another domain with $\mathbf{q}$ and the spin direction along $[1\bar{1}0]$. The second model is a single-domain noncollinear type as depicted in Fig. 1(b), which has tetragonal magnetic symmetry. In the a-b plane this again consists of nearest-neighbor spins being antiferromagnetically arranged, with the moments pointing along an edge direction such as [100]. However, the spins in adjacent layers are orthogonal, and hence the ordered moments alternate along the [100] and [010] directions as one proceeds along the c axis. This model is closely related to the collinear model in that it can be viewed as the coherent superposition of the two separate collinear domains.

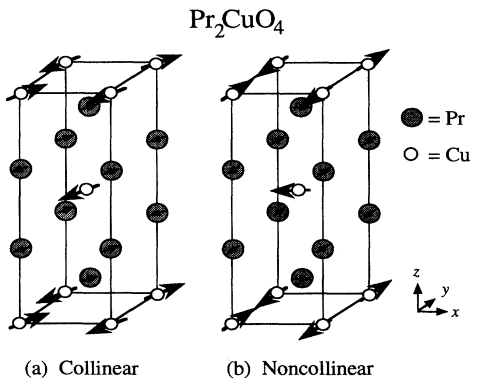

FIG. 1. Spin-structure models for the Cu and Pr ions. (a) Domain of the collinear model, where the spins are aligned parallel or antiparallel along [110]. The antiferromagnetic propagation vector $\mathbf{q} = (\frac{1}{2}\frac{1}{2}0)$ is in the same direction as the ordered spins. (b) Noncollinear model, consisting of a simple antiferromagnetic configuration in the a-b plane, while the spin direction alternates from [100] to [010] as one proceeds along the c axis.

In addition to the Cu ordering, measurements of the temperature dependence of the intensities indicated that the exchange field at the Pr site originating from the ordered Cu spins induces a small moment to order at lower temperatures on the Pr ions. The induced ordering is such that the Pr ions are aligned antiparallel to the neighboring Cu spins along the c axis as illustrated in Fig. 1(b). Low-temperature values for the Cu and induced Pr moments were determined, respectively, to be $0.40 \pm 0.02 \mu_B$ and $0.08 \pm 0.005 \mu_B$. We note that the Pr value is much smaller than the free-ion value of $3.2 \mu_B$; if it were as large as the free-ion value the magnetic intensities at low temperatures would be dominated by the Pr contribution, as was the case in Nd_2CuO_4.[13] The data in Fig. 2 show the temperature dependence of the intensity of the $(\frac{1}{2}\frac{1}{2}1)$ and $(\frac{1}{2}\frac{1}{2}3)$ Bragg peaks. The solid curve is a fit to the higher-temperature data of a power law $(I \propto [1 - T/T_N]^{2\beta})$, which fits the data very nicely for the Cu ordering in other electron superconductor systems.[12] We obtain a value for β of 0.31 ± 0.01 and a Néel temperature of 284 ± 1 K. The overall temperature dependence of the Cu sublattice magnetization is adequately described by a power-law behavior over the full temperature range, while the Pr contribution becomes significant for temperature below ~ 200 K as is obvious from the figure. Note that the experimental data show a very sharply defined ordering temperature, which assures us that the oxygen homogeneity is quite good in this sample. A similar sharp transition is also observed in the 7-g sample. We remark that we have taken rather complete sets of data at selected temperatures, and have also made measurements of the temperature dependence of the intensities for a series of magnetic Bragg peaks. All of our zero-field measurements are in good agreement with those measured previously by other groups,[4,6] and therefore for brevity these detailed results can be found elsewhere.[31]

Returning to the Cu spins, nearest neighbors within the a-b plane are coupled antiferromagnetically, as they are in all the cuprate systems. For the interlayer interaction, the usual bilinear Heisenberg exchange terms between layers cancel on average due to the body-centered tetragonal symmetry, rendering the system fully frustrated. The question then arises as to what higher-order interlayer interactions stabilize the spin structure observed

experimentally. If each domain of the collinear structure is equally populated, as is customarily the case, then the zero-field calculated intensities are *identical* for the two spin configurations. This experimental ambiguity in the spin structures may be resolved by applying a symmetry-breaking field such as a magnetic field, and it is clear that quite different behavior is expected for the two models if the field is applied alternatively in the [110] and [100] directions. Such field-dependent experiments for both directions of applied magnetic field have been carried out for Nd_2CuO_4 and they have shown unambiguously that the Cu spin structure is the noncollinear structure shown in Fig. 1(b).[32] For the other systems investigated in a magnetic field, including the present measurements, the direction of the applied field has been restricted to the [110]-type direction, which is the vertical-field superconducting magnet configuration routinely available. The field-dependent measurements that have been carried out in Sm_2CuO_4 (Ref. 33) and Eu_2CuO_4,[7] as well as for the present system, show a striking similarity to those of Nd_2CuO_4 for fields along the [110] direction. Although these latter measurements are only suggestive of the spin direction, as discussed below, the overall similarity strongly suggests that the correct spin configuration for all these materials is the noncollinear one.

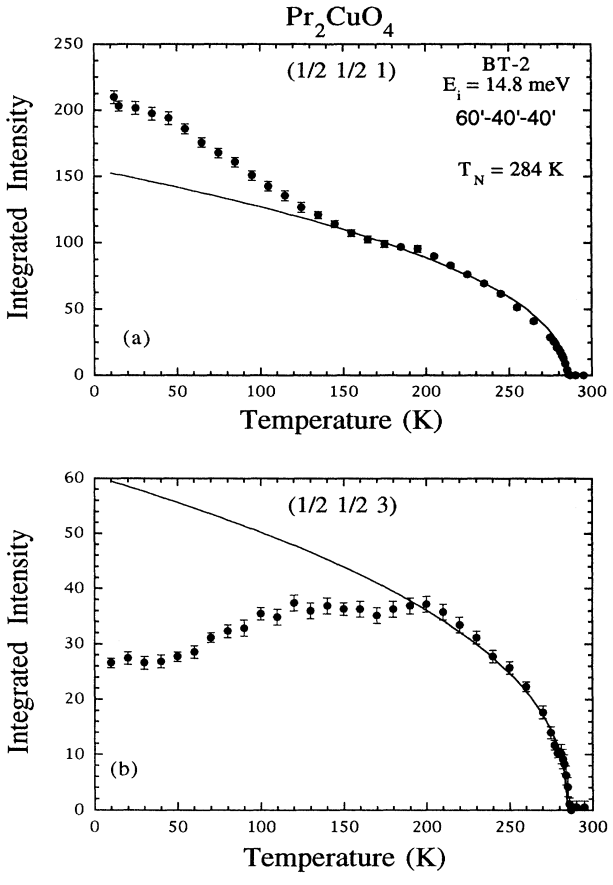

FIG. 2. Temperature dependence of the integrated intensity of the $(\frac{1}{2}\frac{1}{2}1)$ and $(\frac{1}{2}\frac{1}{2}3)$ magnetic Bragg peaks. The solid curve is a fit to a power law for a series of peaks, and describes to a good approximation the contribution of the Cu sublattice magnetization. Below ~200 K an induced Pr moment also contributes to the scattering.

To understand the expected behavior for each model in a field, we first note that the in-plane exchange interactions are huge. Hence laboratory-size fields will have a very small effect on these interactions, and nearest-neighbor spins in the *a-b* plane will remain very close to antiparallel. The principal effect of the magnetic field will be to cause an overall rotation of the spins in each Cu-O layer, and to change the relative orientation of the spin directions in alternate layers. Now consider the effect of a field applied along the [110]-type direction if the noncollinear model is correct. Initially the spins make an angle of $\pi/4$ to **H**, and as the magnitude of the field is increased the spins will rotate into a configuration where the spins are oriented $\sim\pi/2$ to **H** for sufficiently high fields. Since the rotated configuration is energetically different from the zero-field (lower-energy) configuration, removing the field will allow the spins to relax back to their original (noncollinear) configuration. Hence no significant irreversible effects for the intensity as a function of applied field should be expected. For the collinear model, on the other hand, the expected behavior is very different. One domain would have the spins already perpendicular to the field, and there would be little effect on this. The other domain would initially have the spins along the field direction, and these spins would then want to rotate to become perpendicular to **H**, making the second domain identical to the first. Upon removing the field there is no driving force to populate the domains equally again, and thus we would expect strong irreversibility effects to be observed in the field-dependent intensities. Indeed this would be a typical technique to try to produce a single-domain sample, assuming the spin structure were collinear.

Figure 3 shows the intensity variation for the $(\frac{1}{2}\frac{1}{2}1)$ magnetic peak measured as a function of $\mathbf{H}\|[1\bar{1}0]$. The

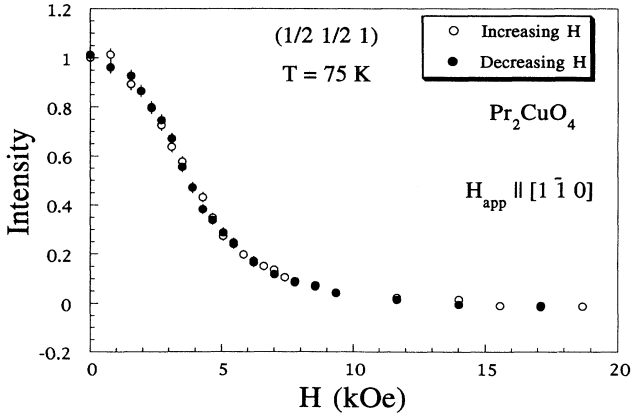

FIG. 3. Variation of the $(\frac{1}{2}\frac{1}{2}1)$ magnetic Bragg peak intensity at $T=75$ K, first with increasing (open circles) and then with decreasing H (solid circles), for H along $[1\bar{1}0]$. No hysteresis effects are observed, as expected for the noncollinear spin model [Fig. 1(b)].

field was first gradually increased (open symbols) and then gradually decreased (solid symbols), at a temperature of 75 K. The background contribution has been subtracted from the measured intensities, which in turn are normalized to unity at zero field. The decrease in intensity to zero with increasing H corresponds to the rotation of the spins into a perpendicular orientation with respect to the applied field. There is an absence of any observable hysteresis effects in the intensity, within experimental error. Identical scans were repeated for a series of temperatures in the range 4.2–250 K. No hysteresis effects were observed in the intensities of any of these scans, thereby strongly suggesting that the noncollinear model is the correct Cu spin structure. This noncollinear structure is also reflected in the configuration of the induced Pr moments as displayed in Fig. 1(b).

Experimentally, no significant hysteresis has been observed in this field configuration for any of the electron systems. For Nd_2CuO_4, it is known that the Cu spin structure is noncollinear,[32] and thus it is likely that the noncollinear model represents the correct spin configuration for all members of the tetragonal T' R_2CuO_4 systems. One possibility is that the noncollinear configuration is stabilized by a weak biquadratic exchange interaction between nearest-neighbor spins in adjacent layers;[34–36] such an interaction would not be expected to play a major role in stabilizing the spin configuration for the related orthorhombic La_2CuO_4 system since the breaking of the tetragonal symmetry gives rise to additional interactions which dominant the interlayer interactions.[37,38] However, the correct identification of the dominant interaction which dictates the ground-state configuration of the T' systems is still an open question.[39,40]

B. Magnetic-field–temperature phase diagram

We have made measurements of the magnetic-field–temperature (H-T) phase diagram for the case of the field **H** applied along $[1\bar{1}0]$; this is exactly the same kind of measurement discussed in the previous section. The field makes an angle of $\pi/4$ with respect to the initial Cu spin direction in the antiferromagnetic (AF) state, and the spins then rotate and orient at an angle $\sim\pi/2$ with respect to the applied field direction. We remark that this "spin-rotated" state, which we designate $\mathbf{R}_\perp$, is directly related to the spin-flop transition that would be expected if the field were directed along the [100] direction, an arrangement that is inaccessible with the magnet system presently available. We thus determined the AF-$\mathbf{R}_\perp$ phase boundary by making field-dependent measurements at a series of temperatures. Figure 4 displays the variation of intensity for the $(\frac{1}{2}\frac{1}{2}1)$ peak with increasing H for a series of temperatures between 4.5 and 200 K. As previously discussed, the decrease in intensity of the $(\frac{1}{2}\frac{1}{2}1)$ peak to zero corresponds to the rotation of the spins into the $\mathbf{R}_\perp$ state. Notice that larger fields are required at lower temperatures to bring the spins into this perpendicular orientation.

For temperatures ≤ 50 K [Fig. 4(a)], the dependence of the rotation angle θ of the Cu spin direction as a function of H can be described by the relation $\sin\theta = H/H_c$, where H_c is the critical field for the transition into the $\mathbf{R}_\perp$ state. This relation is the expected ground-state behavior for a tetragonal system for the case of $\mathbf{H}\|[1\bar{1}0]$,[36,41] and results of the fits to this relation are given by the dashed curves in Fig. 4. However, for higher temperatures, the relation $\tan(\theta) = H/H_c$ provides a better representation of the data, as exemplified by the solid curves in Fig. 4(b). [The relation $\tan(2\theta) = (H/H_c)^2$ is expected for an orthorhombic compound,[38–43] such as La_2CuO_4, in the case where the applied field is at an angle $\pi/4$ from the spin direction.[43]] The underlying reason for the agreement with the field-dependent data in Fig. 4(b) is not yet clear. Moreover, this relation also describes quite well the behavior of the field-dependent intensities in the tetragonal Nd_2CuO_4 and Sm_2CuO_4 compounds at all temperatures down to ~ 5 K,[30] which seems to suggest that this behavior may be a general property for these tetragonal materials, with the behavior given by $\sin(\theta) = H/H_c$ the exception. Values for H_c obtained from the fits will represent the AF-$\mathbf{R}_\perp$ phase boundary in the H-T phase diagram presented below.

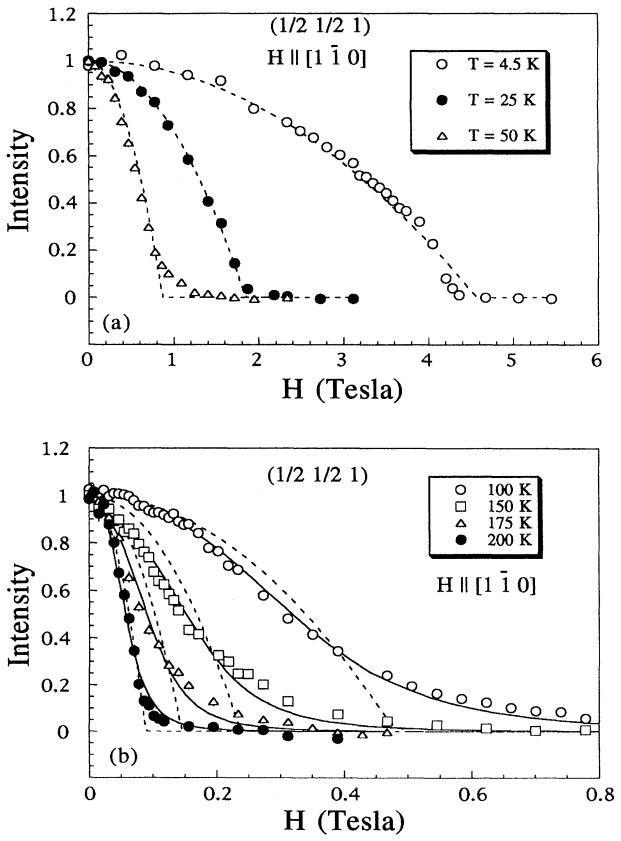

FIG. 4. Field dependence of the $(\frac{1}{2}\frac{1}{2}1)$ peak intensity at a series of fixed temperatures with H along $[1\bar{1}0]$. Dashed curves in the figure and solid curves in (b) are fits to equations described in the text.

For the determination of the upper phase boundary between the $\mathbf{R}_\perp$ state and the paramagnetic state (**P**), we measured the temperature dependence of the $(\frac{1}{2}\frac{1}{2}2)$ peak intensity under a series of applied fields with the results displayed in Fig. 5(a). The data have been corrected for background contribution. These plots are directly related to the square of the Cu order parameter, and the solid curves drawn through these plots are fits to the power law $I(T)=I(0)[1-T/T_N]^{2\beta}$, with $\beta=0.31$ as already discussed. In fact, in the layered CuO systems with no spin reorientations and no rare-earth Cu coupling, such as Sm_2CuO_4,[12] this power-law behavior describes quite well the full temperature range of the data.[3,12] The values of T_N obtained from the fits are plotted in Fig. 5(b) as a function of the applied field, revealing an increase of T_N of $\sim 2°$ under a 7-T field. This is a smaller increase compared to that found in other tetragonal R_2CuO_4 systems, namely, $\sim 3.5°$ for Nd_2CuO_4 ($T_N=276$ K) (Ref. 30) and $\sim 4°$ for Eu_2CuO_4 ($T_N=265$ K).[44] Values of T_N as determined from the power-law fits represent the phase boundary between the $\mathbf{R}_\perp$ state and the **P** state.

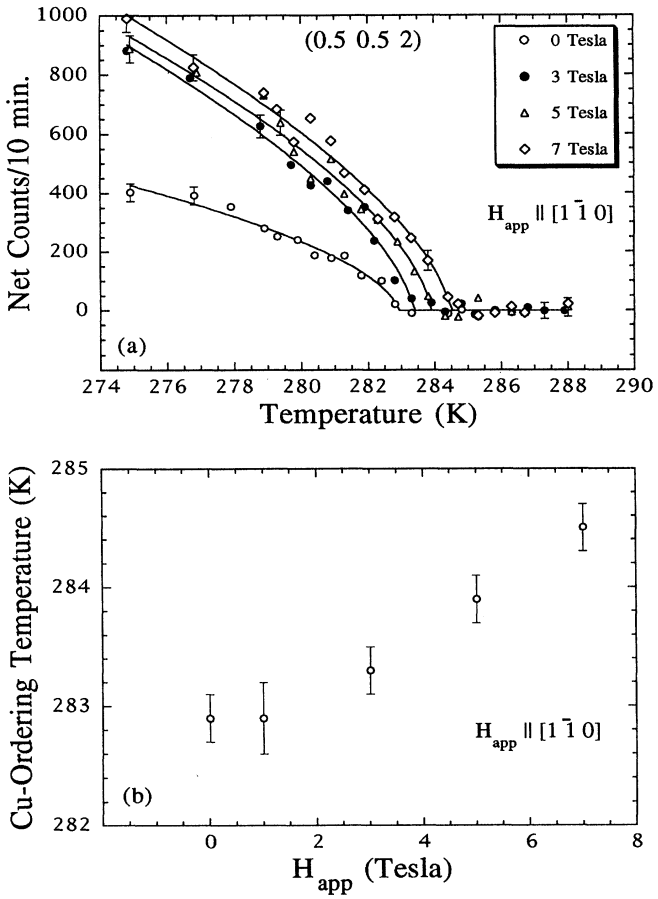

FIG. 5. (a) Temperature dependence of the $(\frac{1}{2}\frac{1}{2}2)$ peak intensity under a series of applied fields along $[1\bar{1}0]$. Solid curves are fits to the power law $I=I(0)[1-T/T_N]^{2\beta}$. (b) Plot of T_N obtained from the power-law fits in (a) vs the applied field H, revealing a shift of T_N of $\sim 2°$ under a 7-T field.

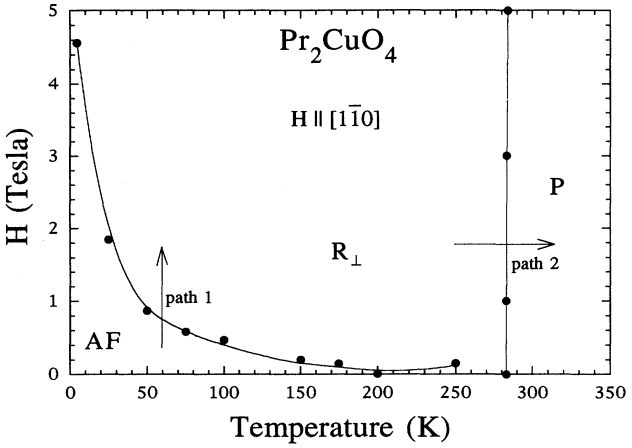

FIG. 6. Magnetic phase diagram for Pr_2CuO_4 in the H-T plane for the case of H applied along $[1\bar{1}0]$, displaying the antiferromagnetic (AF) region, the paramagnetic region (P), and the perpendicular orientation region ($\mathbf{R}_\perp$) where the spins are oriented $\sim\pi/2$ to the applied field. Measurements for the determination of the phase boundaries were made along the paths indicated.

The two measured phase boundaries of the H-T phase diagram for the case of applied field along $[1\bar{1}0]$ are plotted in Fig. 6. It is evident that the AF-$\mathbf{R}_\perp$ phase boundary rapidly increases with decreasing temperature from $T\sim 200$ down to 4.5 K. Above 200 K this field value is very small and it perhaps increases slightly towards the upper $\mathbf{R}_\perp$–**P** phase boundary. Measurements above ~ 250 K become difficult to perform as the intensity for the $(\frac{1}{2}\frac{1}{2}1)$ peak, which has the strongest intensity of all the magnetic peaks, rapidly drops as $T\rightarrow T_N$. Although similar behavior of the AF-$\mathbf{R}_\perp$ transition as determined from neutron diffraction is found in Nd_2CuO_4 and Eu_2CuO_4 for a wide range of temperatures, the spin-rotation transition in these materials decreases again at lower temperatures.[32,44] The Nd-Cu coupling in Nd_2CuO_4 has been mentioned as a possible reason for the decrease in this transition. However, the same cannot be said for Eu_2CuO_4 since the Eu^{3+} ions are nonmagnetic and only a small anomaly has been seen in the order-parameter measurement.[7] It has yet to be determined in Pr_2CuO_4 whether the AF-$\mathbf{R}_\perp$ transition will decrease below 4.5 K, which is the present lowest available temperature. Magnetoresistance techniques have also revealed a monotonic increase of H_c down to $T\sim 150$ K ($H_c\sim 22$ T) in the related orthorhombic La_2CuO_4 system, for the case of the applied field oriented at an angle $\sim\pi/4$ to the ordered spins.[43]

IV. DYNAMICS OF THE Cu SPINS

A. Paramagnetic Cu spin correlations

Measurements of the temperature dependence of the 2D inverse correlation length $\kappa_{2D}=1/\xi_{2D}(T)$ have been

made in a number of the layered cuprate materials.[4,8,17,45] We have carried out more detailed measurements of κ_{2D} in Pr_2CuO_4 compared to previous data, in the temperature range $T_N < T \leq 475$ K where the spins between CuO layers are weakly correlated. In this regime the system is expected to exhibit the behavior of a 2D $S=\frac{1}{2}$ quantum Heisenberg antiferromagnet (QHAF),[15–18] which is a model of interest in studies of quantum magnets. Analytic results are not yet available for this model, but approximate theoretical methods and simulations have been effectively employed to calculate the spin-spin correlation length ξ_{2D} as a function of temperature.[15]

Due to the 2D nature of the magnetic interactions above T_N, the scattering in reciprocal space forms rods of intensity, and the width of these rods is a direct measure of κ_{2D}. Data were collected on the ~7-g single crystal using an incident energy $E_i=28$ meV and collimations of 60′ before the monochromator, and 20′-20′ before and after the sample. Scans were taken across the $(\frac{1}{2},\frac{1}{2},l)$ rod, and we chose $l=0.343$ since this is the condition where the final neutron wave vector $\mathbf{k}_f$ is parallel to the 2D scattering rod, allowing an experimental energy integration from approximately $-k_BT$ up to the incident neutron energy $+E_i$. For the temperature range of interest the dominant contribution to the dynamic 2D spin fluctuations is contained within this energy range, and thus this technique will provide an accurate measure of ξ_{2D} as demonstrated in the related systems.[8,18] Figure 7 shows data obtained at three different temperatures, and the solid curves are fits to an intrinsic Lorentzian convoluted with the (Gaussian) resolution function. The small slope to the background arises from the background variation with scattering angle. The peak in Fig. 7(a) has a width which is close to the instrumental wave-vector resolution, while at higher temperatures the intrinsic widths obviously increase, reflecting the reduction in the spin-correlation length with increasing temperature.

The integrated intensities of the 2D peaks are plotted versus temperature in Fig. 8(a). The rod intensity increases steadily as T_N is approached from above, reaches a maximum at around T_N, and then decreases below T_N. Similar behavior is also observed in Nd_2CuO_4 (Ref. 4) and

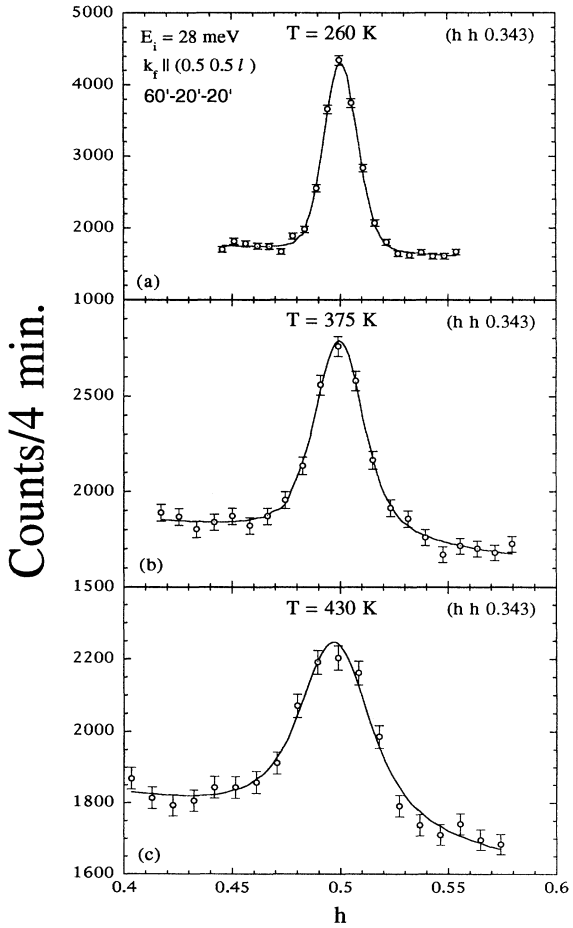

FIG. 7. Energy-integrated scans across the magnetic rod $(\frac{1}{2}\frac{1}{2}l)$ at a series of temperatures. The solid curves are fits to a convolution of a Lorentzian function with a Gaussian resolution function. A sloping background is also included in each fit.

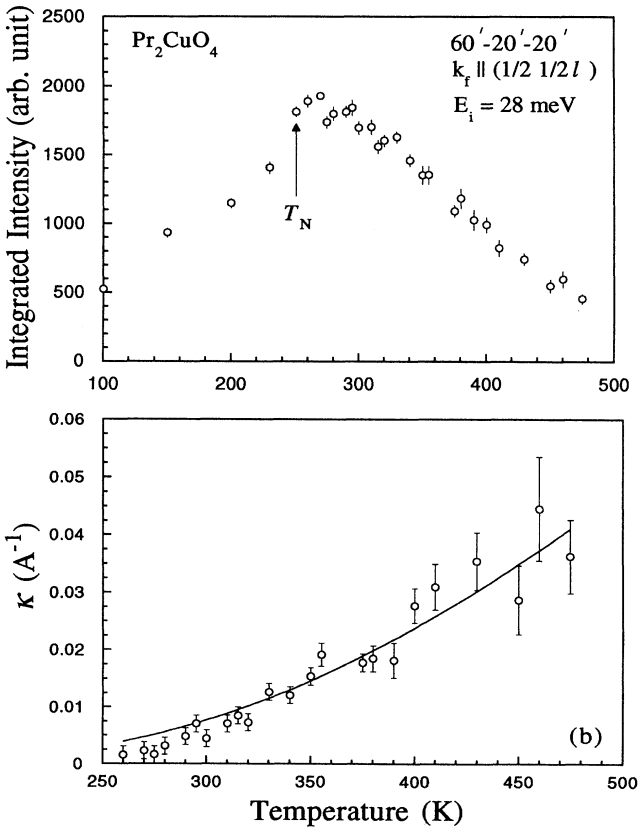

FIG. 8. (a) Temperature dependence of the integrated intensity for the 2D rods as shown in Fig. 7. The three-dimensional ordering temperature for this crystal is 251 K. (b) Temperature dependence of the inverse correlation length for the Cu spins. The solid curve is a result of the fit using Eq. (1).

La_2CuO_4,[45] for example, and is consistent with a crossover from 2D to 3D behavior; below T_N there is a removal of intensity from the 2D rod as the 3D Bragg peaks appear and grow in strength. The gradual variation of the rod intensity with temperature has been interpreted as an indication of the 3D transition driven by weak interlayer coupling. However, it has also been suggested that for the case of the tetragonal R_2CuO_4 materials a crossover to a 2D xy model is first expected to occur as $T \rightarrow T_N$ from above, driven by the anisotropy in the Heisenberg exchange interactions, and this would be followed by a crossover to a 3D xy system.[4,38] For the level of data available in this system so far, either scenario is consistent with the observations.

Figure 8(b) shows the temperature dependence of the measured κ_{2D}, where the 2D correlation length evolves from a few lattice constants at $T=475$ K up to ~ 80 lattice constants at $T=260$ K. The experimental data are in good agreement with the data obtained by other groups[4,8] where they overlap. The solid curve is a fit to the prediction based on the renormalized classical theory of the 2D quantum nonlinear σ model given by[15–18]

$$\xi_{2D}=0.493a \exp\left[\frac{1.15J}{k_BT}\right]\left[1-0.43\left[\frac{k_BT}{J}\right]+O\left[\frac{k_BT}{J}\right]^2\right], \quad (1)$$

where a is the lattice parameter and J is the nearest-neighbor exchange constant as determined below. The model is assumed to describe the behavior of the 2D QHAF in the long-wavelength limit at low temperatures ($k_BT \ll J$), and we have kept only the first two terms in the fit. The model provides an adequate representation of the data at higher temperatures, as has been found for the other layered CuO materials.[4,8,18,45] However, the 2D QHAF model exhibits long-range order only at $T=0$, and thus the systematic deviations observed as T_N is approached are expected as the crossover to 3D behavior occurs. The present measurements, though, do not have sufficient resolution and/or intensity to obtain more detailed information about the expected crossover to 2D xy behavior as the correlation length exceeds ~ 70 lattice constants,[4,38] or to directly observe the crossover to 3D behavior.

B. Cu spin waves

Since the noncollinear spin structure of the tetragonal R_2CuO_4 compound is comprised of four sublattices, the dispersion relations of the Cu spin waves, in general, consist of four branches.[46] To leading order, all of the four branches propagating in the a-b plane are degenerate and highly dispersive, with a spin-wave velocity c which is expected to be very large as found in the other cuprate materials such as La_2CuO_4 ($c=0.85\pm0.03$ eV Å).[47,48] Due to the very steep nature of the dispersion propagating in the a-b plane, it was necessary to make measurements of the spin-wave velocity with the constant-energy technique, in order to try and resolve the $+q$ and $-q$ spin-wave branches. All of the spin-wave velocity measurements were performed with a configuration where $\mathbf{k}_f$ was fixed. Various collimations were used along with either a PG or a Cu monochromator as necessitated by resolution and instrumental considerations.

Figure 9 shows representative constant-E scans across the 2D scattering rods for a series of energies. Data in Fig. 9(a) were taken at a temperature of 265 K, while those in Figs. 9(b) and 9(c) were taken at $T=10$ K. As far as the temperature dependence is concerned, we found that for energy transfers above ~ 10 meV the behavior of the spin-wave intensities as a function of temperature is well described by linear spin-wave theory, and aside from the thermal factor no significant differences could be observed from room temperature (above T_N) to 10 K. In Fig. 9(a), a single resolution-limited peak can be observed at $E=10$ meV from the scan across (1.5 1.5 0.2). A PG(002) monochromator was used to obtain these data, and the instrumental resolution was not

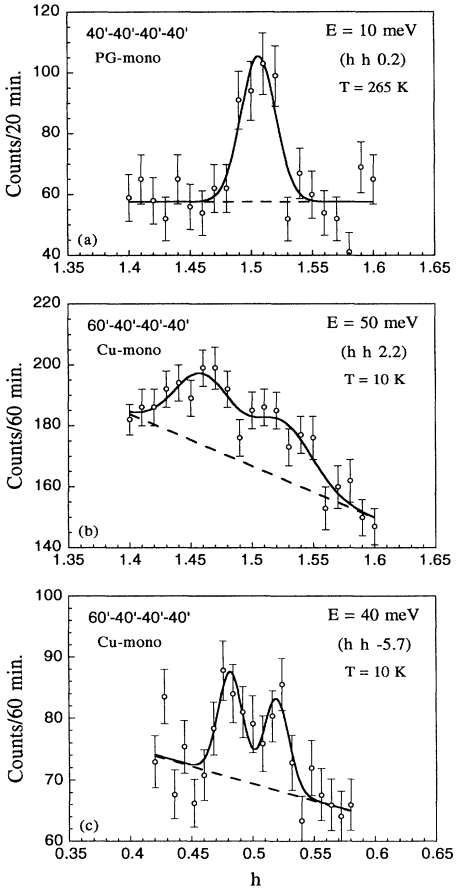

FIG. 9. Typical constant-energy scans for 10, 50, and 40 meV. Solid curves are results from Gaussian fits and dashed curves are the fitted background. The two clearly resolved peaks shown in (b) and (c) correspond to the $+q$ and $-q$ magnon branches, which are not resolved in (a) because of the closer spacing of the spin waves and coarser instrumental resolution employed.

sufficient to separate the $+q$ from the $-q$ magnon branches. To improve the instrumental resolution, a Cu(220) monochromator was employed for the higher-energy transfer data, where in addition the magnons at $\pm q$ will be further apart. The data obtained in the vicinity of $\mathbf{Q}=(1.5\ 1.5\ 2.2)$ for an energy transfer of 50 meV are displayed in Fig. 9(b). The solid curve is a fit to two resolution-limited spin waves, and the sloping background (dashed line) is due to the scattering angle decreasing with decreasing Q. Figure 9(c) shows data obtained for $(0.5\ 0.5\ -5.7)$ at $E=40$ meV. This position in $\mathbf{Q}$ was chosen to achieve optimal instrumental focusing for the triple-axis spectrometer, and the peaks corresponding to the two spin-wave branches are clearly resolved. Our value for the spin-wave velocity is $c=0.85\pm0.08$ eV Å, which corresponds to a nearest-neighbor exchange constant J of 130 ± 13 meV. This compares reasonably well with that derived from Raman scattering in the sister compound Nd_2CuO_4.[14]

To investigate the spin-wave scattering at lower energies and to search for the expected spin-wave gaps, we used an instrumental configuration where the initial neutron wave vector $\mathbf{k}_i$ was fixed. Figure 10 shows the energy dependence of the integrated intensities of the magnon peaks measured with the constant-E scan across $(\frac{1}{2}\frac{1}{2}1.5)$ at $T=10$ K. The data have been corrected for resolution effects arising from the variation in $\mathbf{k}_f$. The solid curve in the figure is just a guide to the eye. At this wave vector, the spin-wave spectrum is expected to exhibit two energy gaps.[46] One such gap is observed around 5 meV in the figure. We have made identical measurements across several other l points along $(\frac{1}{2}\frac{1}{2}l)$, and from the behavior of the intensity variation with l, it can be established that this energy gap corresponds to the reduced xy-anisotropy constant $\alpha_\parallel=(J-J^{xy}/J)$ of the nearest-neighbor Heisenberg exchange interaction given by $E_g=4J(\alpha_\parallel/2)^{1/2}$. The measured size of the gap of ~5 meV was also observed from neutron-scattering measurements[49] in the sister compound Nd_2CuO_4, but is much higher than that reported from magnetic resonance measurements,[50] which is ~0.5 meV. In the related La_2CuO_4 system this gap is found to be ~2.5 meV.[51] Our measured gap yields a reduced anisotropy constant $\alpha_\parallel=2\times10^{-4}$.

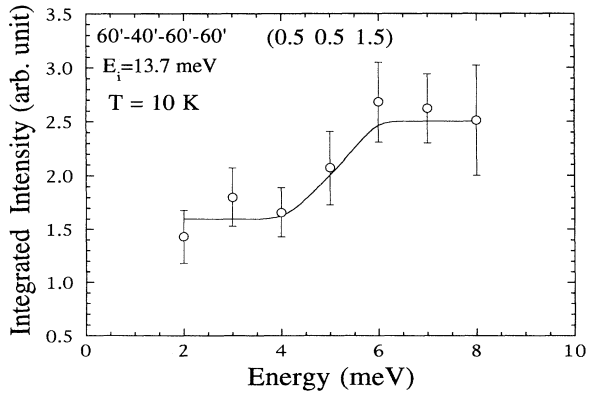

FIG. 10. Variation of the spin-wave intensity with energy at $(\frac{1}{2}\frac{1}{2}1.5)$. The solid curve is a guide to the eye. The data reveal an energy gap of ~5 meV.

There is still a well-defined peak from the spin-wave scattering at 2 meV, suggesting that the other spin-wave gap is at an energy substantially less than 2 meV. Measurements at lower energies could not be performed because of the significant contribution from incoherent elastic scattering. This other gap is related to the interplanar biquadratic exchange constant, which is at least 6 orders of magnitude smaller than the in-plane exchange constant J. A more accurate determination for the biquadratic exchange constant would be desirable in order to ascertain whether it could explain the observed T_N and spin structure in the tetragonal R_2CuO_4 class of materials. This, however, would require much better instrumental resolution than presently available. It has been suggested that a measurement of the biquadratic exchange constant is possible via light scattering experiments,[52] but we are not aware of any experimental work carried out to date.

V. DYNAMICS OF THE Pr SPINS

A. Magnetic excitons

The crystal-field ground state of the Pr ions has been determined to be a singlet via inelastic neutron scattering, with the doubly degenerate first excited state lying at an energy ~18 meV above the ground state.[20–23] The singlet ground state, which is a nonmagnetic state, is also supported by magnetic susceptibility[10] and specific-heat[11] measurements. Spontaneous magnetic ordering of the Pr ions in this case can occur only if the exchange interactions are strong enough to overcome the quenching of the magnetic moment by the crystal field,[25] and for Pr_2CuO_4 we are in the opposite limit of having weak exchange compared to the crystal-field splitting. It is known that for such systems the elementary collective excitations are conveniently described as linear combinations of the single-ion crystal-field transitions propagating throughout the lattice.[25] These collective modes, known as *magnetic excitons,* exhibit dispersion due to the exchange coupling between the magnetic ions. Magnetic excitons of a singlet-ground-state system have been studied extensively for Pr metal,[25–27,53–54] ferromagnetic fcc-stabilized Pr (Refs. 55 and 56) and Pr_3Tl.[55,57] Well-defined magnetic excitons with pronounced dispersion have been observed in the ordered as well as in the paramagnetic regimes in these materials.

As can be seen from the crystal structure shown in Fig. 11, the basic Pr unit cell has a body-centered tetragonal symmetry with a two-ion basis. The corresponding Brillouin zone for a body-centered tetragonal lattice with $c>a$ is also shown in the figure. The unit cell of the Pr ions can also be looked upon as two interpenetrating identical sublattices, where the surrounding of the two ions belonging to each sublattice are equivalent except for an inversion. The basic model Hamiltonian for the Pr ions is assumed to have the following form:[26,27]

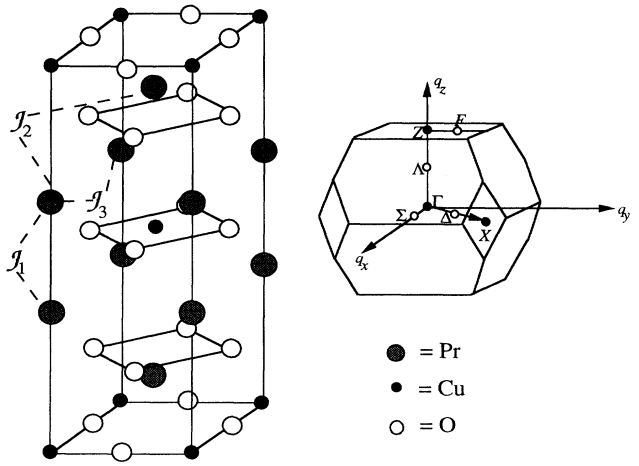

FIG. 11. Crystal structure of Pr_2CuO_4, with the various Pr-Pr exchange constants indicated, and the Brillouin zone for the body-centered tetragonal lattice where $c > a$.

$$H = \sum_i V_i^c - \sum_{i>j} J(\mathbf{r}_i - \mathbf{r}_j)\mathbf{J}_i \cdot \mathbf{J}_j - \sum_{i>k} J'(\mathbf{r}_i - \mathbf{r}_k)\mathbf{J}_i \cdot \mathbf{J}_k \ , \quad (2)$$

where the first term corresponds to the single-ion crystal-field potential and the rest are terms arising from the exchange interactions as indicated in Fig. 11. The quantities $J(\mathbf{r}_i - \mathbf{r}_j)$ and $J'(\mathbf{r}_i - \mathbf{r}_k)$ are, respectively, the intrasublattice and the intersublattice exchange constants between ions with angular momentum $\mathbf{J}$. A bilinear Heisenberg exchange interaction has been assumed for simplicity, and is found to provide a good description of the measurements. If we denote the ground state wave function by $|G\rangle$ and the first excited state by $|E\rangle$, then at low temperatures the only excitons that propagate are those involving the $|G\rangle - |E\rangle$ transition since nearly all the Pr ions are in the crystal-field ground state.

Within the random-phase approximation (RPA), the dispersion relation for the $|G\rangle - |E\rangle$ exciton modes in the paramagnetic state at $T = 0$ is[26,27]

$$E(\mathbf{q}) = [\Delta^2 - 2M^2\Delta\{J(\mathbf{q}) \pm |J'(\mathbf{q})|\}]^{1/2} \ , \quad (3)$$

where $J(\mathbf{q})$ is the Fourier transform of the exchange constant. The parameter Δ is the crystal-field splitting between the ground state and the first excited state in the absence of any exchange interactions and M denotes the matrix element for the component of the angular momentum $\langle G|J_r|E\rangle$, where $r = x,y$. The dispersion relations in Eq. (3) consist of two branches, the "acoustic" and "optical" modes, as expected from the two-ion basis in the Pr unit cell.

B. Low-temperature measurements

The $|G\rangle - |E\rangle$ magnetic exciton modes that dominate the dynamics of the Pr ions at ~ 18 meV have a strong cross section, thereby assisting us in obtaining high-quality data. In contrast to the Cu spin waves, these modes are relatively flat and all measurements were therefore made via the constant-Q technique. For the case when $l = 0$, the dynamical structure factor in the neutron cross section predicts that only the acoustic mode will be observable, and Fig. 12 shows representative scans for magnetic excitons propagating in the [110] direction. Indeed only single well-defined peaks are observed for this case. The solid curves in the figure are fits to a Gaussian function, and reveal that any intrinsic widths are too small to measure at low temperature. The intensities of these peaks vary with Q in agreement with the expected dynamical structure factor $|f(\mathbf{Q})|^2M^2\Delta/E(\mathbf{q})$, where $f(\mathbf{Q})$ is the Pr^{3+} form factor, signifying that the measured peaks are indeed scattering from the acoustic excitons. The peak at (110) [Fig. 12(a)] represents the exciton mode at the center of the Brillouin zone, Γ, while the one at (1.5 1.5 0) [Fig. 12(b)] represents the mode at the zone boundary. Comparison between the two peaks clearly reveals a shift in the peak position from 19.1 meV at the zone center down to 17.9 meV at the zone boundary, directly demonstrating a dispersion of 1.2 meV.

The measured dispersion relations for the acoustic magnetic excitons are shown in Fig. 13 for propagation along [110] and [100]. The data cover more than one Brillouin zone, where the boundaries are indicated by the vertical dashed lines. It can be seen that the periodicity

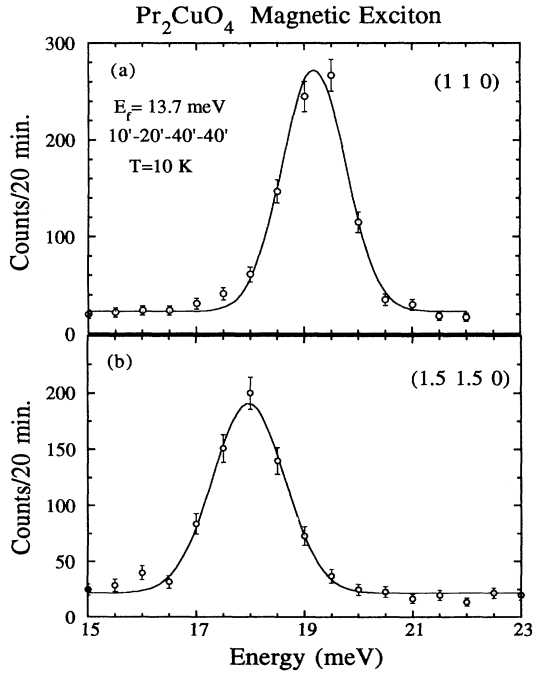

FIG. 12. Constant-Q scans of the acoustic magnetic exciton peaks propagating in the [110] direction. Solid curves are fits to a Gaussian (resolution) function. The peak at (1 1 0) corresponds to the zone center mode (top) while the peak at (1.5 1.5 0) corresponds to the zone boundary mode (bottom).

of the excitons is in agreement with that expected for the reciprocal lattice of the Pr chemical unit cell. The labels Δ and Σ denote directions of high lattice symmetry from the zoner center, Γ, whereas the label F represents the direction along the face of the Brillouin zone as indicated in Fig. 11. Anticipating that the dominant exchange interactions involved are relatively short range in nature, we have analyzed the data by including up to third-neighbor exchange constants. The solid curves drawn through the data in Fig. 13 are calculated with the following parameters: $\Delta=18.0$ meV, $2M^2J_1=0.7$ meV, $8M^2J_2=0.8$ meV, and $8M^2J_3=-0.8$ meV, where J_i are the exchange constants between ith neighbors. As indicated in Fig. 11, J_2 corresponds to the coupling between those Pr layers that are separated by oxygen layers, and J_3 is a measure of the coupling between nearest-neighbor ions within the a-b plane. We remark that these constants can be directly determined with the use of Eq. (3) by subtracting the measured $E(\mathbf{q})$ for the [100] direction from the [110] direction at selected scattering vectors, so there is not much relative ambiguity in their values; the statistical uncertainties are $\sim\pm0.05$ meV. The remaining parameter J_1, which represents the coupling between those Pr layers that are separated by the Cu-O layers, can then be obtained from a two-parameter fit. It is evident that Eq. (3) provides excellent representations of the data in Fig. 13.

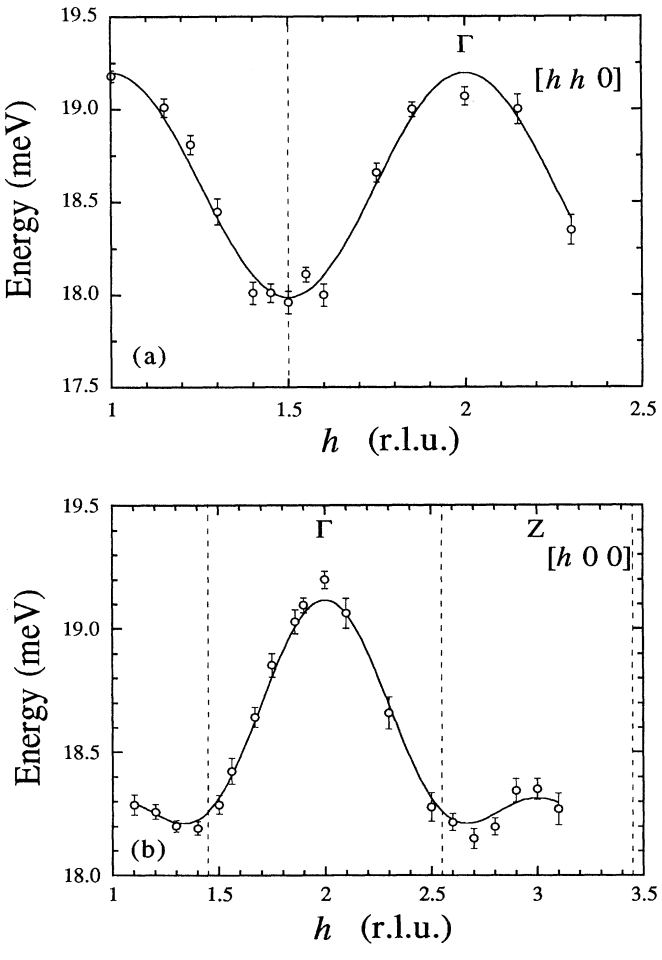

FIG. 13. Measured low-temperature dispersion relation of the Pr^{3+} acoustic exciton mode in Pr_2CuO_4, propagating in the [110] (top) and in the [100] (bottom) directions. The solid curves are fits for the exciton dispersion relations as explained in the text.

The above analysis for the acoustic magnetic excitons yields nonzero values of J_1 and J_2, both of which are interplanar exchange constants. Consequently, the excitons propagating along the c axis should exhibit dispersion, and we now turn our attention to measurements for excitations for which $l\neq0$. Figure 14 shows representative constant-Q scans taken at a series of Q along [00l] and along [hh6]. Two peaks can be observed as a result of scans at (0 0 6) and (1 1 6), both of which are zone center points, as displayed in Figs. 14(a) and 14(c), respectively. The peak with the higher intensity is centered at ~19.2 meV while the other is positioned at ~16.9 meV. The latter should be the "optical" mode of the magnetic excitons since this mode will contribute to the cross section for scattering vectors where $l\neq0$. For values of $\mathbf{q}$ away from the zone center, the energy separation between the two peaks narrows as illustrated in Figs. 14(b) and 14(d) for scans at (0 0 6.5) and at (0.9 0.9 6). The available instrumental resolution could not cleanly resolve the two peaks for some directions of $\mathbf{Q}$. Notice that the intensity of the optical exciton peak increases whereas that of the acoustic exciton peak decreases as $\mathbf{q}$ varies away from the zone center position. This behavior for the intensity of the two peaks as a function of wave vector $\mathbf{q}$ is expected from the theoretical structure factor for each mode. The combined integrated intensity of both peaks also varies with $\mathbf{Q}$ in agreement with the calculated dynamical structure factor.

Figure 15 shows the measured energies of the observed exciton peaks for a series of scattering vectors $\mathbf{Q}$ varying along the [00l], [h06], and [hh6] directions. The points where only a single value of energy is plotted at a given $\mathbf{Q}$ is due to the inability of the instrumental resolution to resolve the two expected peaks. The solid curves are calculated dispersion relations for the two branches as given by Eq. (3), using the previously determined parameters, while the dashed curve in Fig. 15(c) is a guide to the eye for the measured lower-energy dispersion relation. The overall agreement between theory and experiment in Figs. 15(a) and 15(b) is quite satisfactory. We remark that we have observed a small additional peak at ~16 meV at some scattering vectors $\mathbf{Q}$ in the directions of [00l] and [h06]. We believe this peak is a phonon branch based on its temperature dependence and also on measurements of the phonon dispersion relations in Pr_2CuO_4 and Nd_2CuO_4, which indicate a phonon mode at the observed energy.[58] Interference from these small peaks may be the origin of these small discrepancies. The disagreement between the lower-energy excitation in Fig. 15(c) with the expected optical branch, on the other hand, probably reflects an interaction with another type of excitation, such as phonons; the large value of the or-

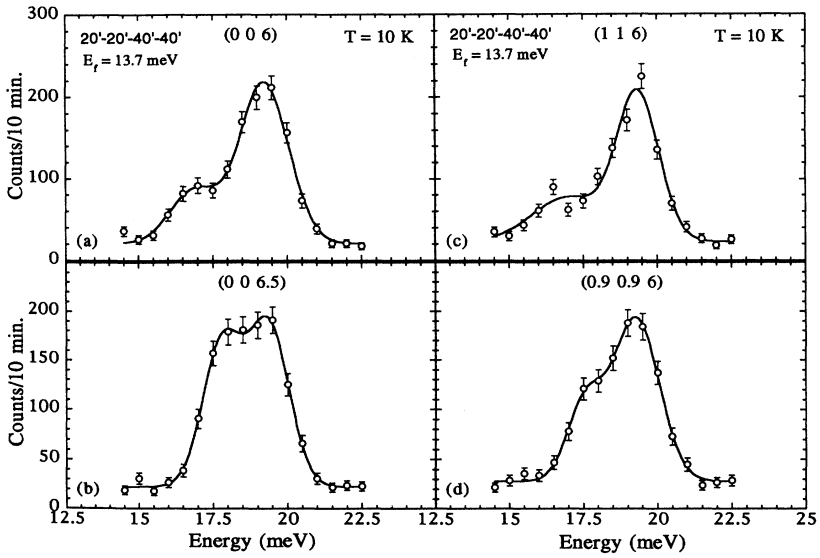

FIG. 14. Examples of constant-Q scans taken for Q along [00l] in (a) and (b) and along [hh6] in (c) and (d). The separation in energy of the two peaks corresponding to the acoustic and optical exciton modes is furthest apart at the zone centers, (0 0 6) and (1 1 6).

bital momentum of the Pr ions ($L=5$) typically leads to strong exciton-phonon coupling. Exciton-phonon interactions have been observed in Pr metal under an external magnetic field,[27,53,54] and indeed there are indications of an interaction observed in Raman scattering measurements.[59]

We note that the Cu spins in this crystal have already ordered at $T_N=251$ K and the ordering induces a small moment at the Pr sites. Such an induced moment is only possible via an admixture of higher J multiplets and/or if the Cu exchange field on the Pr ions mixes one of the Pr excited states into the ground state. The singlet state would then shift in energy and the degeneracy of the doublet states would be lifted.[20,25] The widths of the magnetic peaks for the acoustic excitons are essentially instrumental in origin signifying that if such a splitting exists it is too small to observe in the present experiments; the value of the Pr ordered moment is only $\sim 0.08\mu_B$, which corresponds to an admixture of only a few percent.[20] We thus believe that the dispersion relations in the paramagnetic state given by Eq. (3) adequately describe our data to a good approximation.

The significant dispersion of the crystal-field excitations as demonstrated here provides direct evidence of substantial exchange interactions between the Pr ions. Such an interaction has been previously deduced from neutron-diffraction,[12,13] susceptibility,[9,10] and specific-heat[11] measurements of the rare-earth ordering in the tetragonal R_2CuO_4 materials, as well as in the Ce-doped superconducting compounds $Nd_{1.85}Ce_{0.15}CuO_4$ and $Sm_{1.85}Ce_{0.15}CuO_4$, where the Cu spins are not ordered. Dipolar interactions are orders of magnitude too small to explain the observed T_N for the rare-earth ordering. The fact that the undoped materials are insulators suggests that the interactions are likely of the superexchange type. The observed dispersion of the excitons along the c axis here in Pr_2CuO_4 signifies that these interactions are mediated through the CuO layers. Since in the doped system it is the same CuO planes are also involved in the formation of superconductivity, this may provide insight into the nature of the superconducting state for the tetragonal R_2CuO_4 systems, where the Cooper-pairing occurs in the presence of these magnetic interactions. It will be interesting to investigate the magnetic excitons in doped crystals when samples of sufficient size become available.

C. Temperature-dependent measurements

For finite temperatures, the exciton dispersion relation in Eq. (3) can be modified to include a temperature-dependent renormalization factor $R(T)$ in the exchange term.[25,26,60,61] In a simple RPA theory, $R(T)$ is merely the difference in Boltzmann population factors between the ground state n_G and the excited states n_E, which is reasonably approximated (neglecting the dispersion and higher-energy crystal-field levels) by[25,26]

$$R(T)=n_G-n_E=\frac{1-\exp(-\Delta/k_BT)}{1+2\exp(-\Delta/k_BT)}\ , \tag{4}$$

where Δ is the splitting between the ground state and the doubly degenerate excited state in the absence of exchange interactions. A more accurate derivation is given by self-consistent RPA theory,[60-61] in which effects of dispersion are explicitly included, but in the present case the relative exchange to crystal-field energy is sufficiently small that a more elaborate analysis is not warranted. As a result of this renormalization factor, the dispersion of the exciton modes would become essentially flat as k_BT becomes comparable to Δ (≈ 210 K). If the ratio $|2M^2\{J(\mathbf{q})\pm|J'(\mathbf{q})|\}/\Delta|$ is less than unity for all wave vectors $\mathbf{q}$, the system will remain in a Van Vleck paramagnetic state down to $T=0$.[25] For Pr_2CuO_4, the maximum ratio is 0.16 so that the Pr system by itself will

not display spontaneous order at low temperatures.

In order to investigate the temperature-dependent effects on the dispersion relation of the magnetic excitons, two acoustic modes propagating along [100] were selected for detailed investigation: the zone center mode at (2 0 0) and the mode at (1.4 0 0), which is near the zone boundary. These modes have, respectively, the maximum and the minimum energy for the measured acoustic branch. Figure 16 shows representative constant-**Q** scans of the mode at (2 0 0) measured at three temperatures. The solid curves are fits to a Gaussian function and the dashed curves are the backgrounds included in the fits. The intensities of the peaks decrease, they shift, and the widths increase with increasing temperature. However, close inspection of the data in Fig. 16(b), made at $T=100$ K, reveals an additional small peak at ~ 17 meV. This additional scattering is phonon in origin,[58] and indicates some of the difficulties in correctly identifying and isolating the magnetic scattering. We note that phonon scattering increases with increasing temperature via the Bose thermal population factor, while crystal-field scattering out of the ground state decreases in intensity as the ground-state occupation is depleted. The linewidths of these excitations also increase with increasing T, and thus we were able to observe this shoulder only over a limited range of temperature (from ~ 100 to 200 K). No evidence of phonon contamination was observed for the exciton mode at (1.4 0 0).

Figure 17 shows the temperature evolution of the full width at half maximum and integrated intensity for both exciton modes. For $\mathbf{Q}=(2\ 0\ 0)$ these data are from single-Gaussian fits due to the difficulties as just discussed. It is evident that the widths for both peaks increase with increasing temperature and are comparable in size in the temperature range $15 \leq T \leq 150$ K. For higher temperatures, however, the width of the (2 0 0) peak increases more rapidly than that of the (1.4 0 0) peak, and

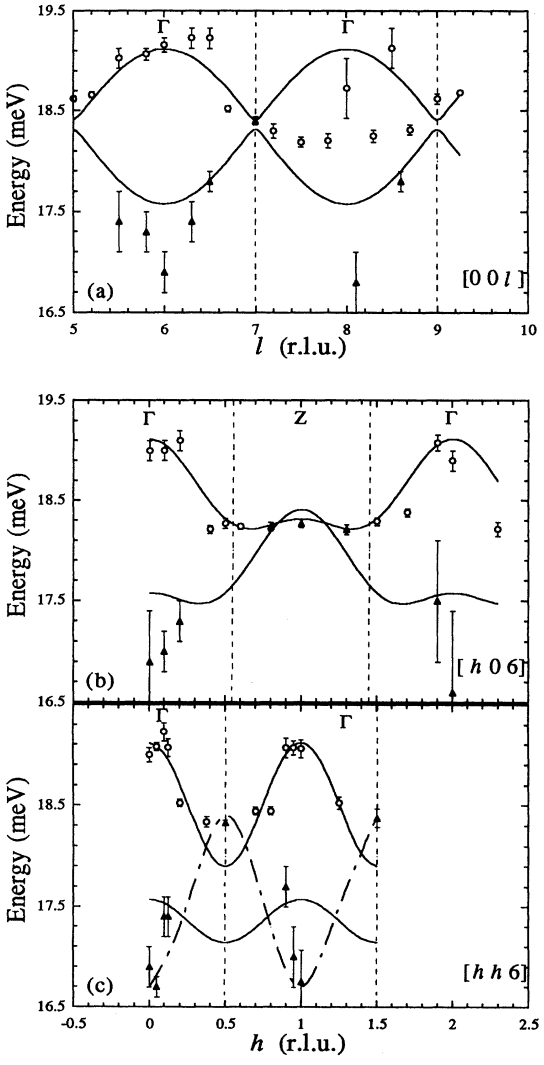

FIG. 15. Magnetic exciton dispersion relations of the acoustic mode (open symbols) and the optical mode (solid symbols) in Pr_2CuO_4, as measured with **Q** along (a) [00*l*], (b) [*h*06], and (c) [*hh*6]. Points where only a single energy is plotted for a given scattering vector are due to the inability of the available instrumental resolution to separate the two peaks. Solid curves are the calculated dispersion relations as explained in the text, while the dashed curve is a guide to the eye for the measured lower-energy dispersion relation.

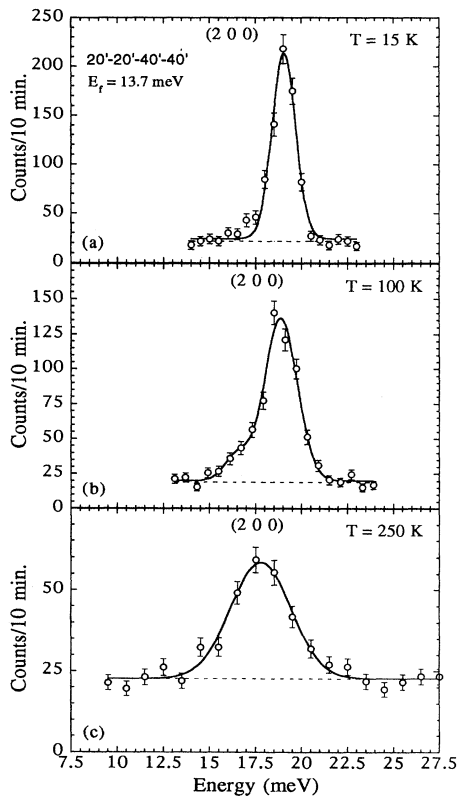

FIG. 16. Constant-**Q** scans for the acoustic mode at (2 0 0) taken at three temperatures.

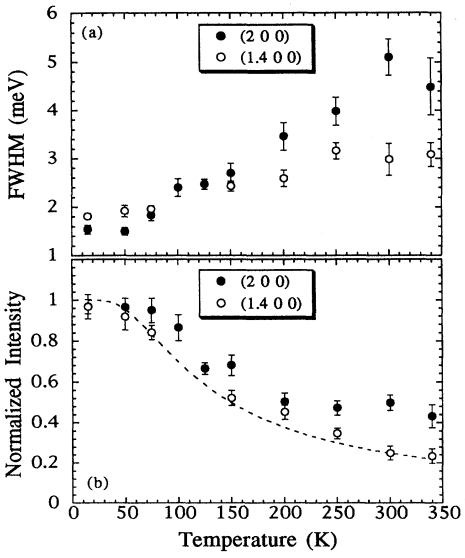

FIG. 17. (a) Temperature dependence of the full width at half maximum obtained from fitting the data such as in Fig. 16 by a single Gaussian peak. (b) Normalized temperature dependence of the integrated intensity of the fitted peaks. The dashed curve is the calculation from Eq. (4).

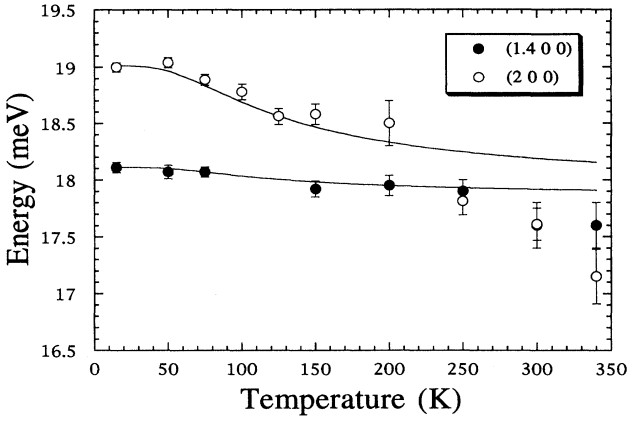

FIG. 18. Temperature dependence of the energy of the acoustic exciton modes at (1.4 0 0) and (2 0 0). Data for the mode measured at (2 0 0) in the temperature range $100 \leq T \leq 200$ K are obtained from a two-peak fitting. Solid curves are the calculated exciton energies using Eqs. (2) and (4) in the text.

we believe that this is caused by the phonon contribution to the scattering. Comparison between the temperature dependence of the integrated intensities of the peaks for the two modes is shown in Fig. 17(b), normalized to unity at $T=0$. The behavior of the normalized integrated intensity for the peak measured at (1.4 0 0) is well described by the function $R(T)$ given by Eq. (4), whereas the (2 0 0) exhibits some additional intensity at higher T, which we again attribute to the phonon. We conclude that the magnetic part of the scattering is well described by the theory.

The behavior of the energies of magnetic excitons as a function of temperature is plotted in Fig. 18 for the modes at (2 0 0) and (1.4 0 0). Results for the exciton mode at (2 0 0) in the temperature range $100 \leq T \leq 200$ K were obtained from two-peak fits to the data. The solid curves are the calculations based on the parameters obtained from the low temperature data and Eq. (4). Below ~ 200 K the data are in good agreement with the simple RPA theory. At higher temperatures both energies are approximately equal, indicating that the mode now has little dispersion, as theoretically expected. Both observed energies fall below the theory; however, the value of Δ itself should decrease with increasing temperature due to ordinary thermal expansion, and this is the likely explanation for the observed behavior at elevated temperatures. Hence we conclude that the simple renormalized RPA theory provides a good overall description of these excitations over the entire temperature range explored.

VI. DISCUSSION

The results reported here present a better understanding of the microscopic magnetic properties of Pr_2CuO_4, which in turn should contribute to a general understanding of magnetism in the class of tetragonal R_2CuO_4 materials (R = rare earth). In fact, some of the magnetic behavior of Pr_2CuO_4 observed in our measurements is likely to be exhibited by other members of the tetragonal R_2CuO_4 materials. One of the most important aspects is the significant dispersion exhibited by the Pr magnetic excitons, particularly along the c axis, which directly indicates that the Pr subsystem is not electronically isolated from the CuO planes. Indeed substantial rare-earth exchange interactions appear to be a general property of these electron-doped systems, as supported, for example, by the relatively high (6 K) rare-earth ordering temperatures observed in both Sm_2CuO_4 (Refs. 9 and 12) and $Sm_{1.85}Ce_{0.15}CuO_4$,[9] while the dipolar interactions are several orders of magnitude too small to account for T_N. It will be interesting to pursue similar inelastic measurements on doped samples to see how superconductivity affects the magnetic excitons in particular, and the rare-earth magnetism in general.

The basic features of the Cu spin dynamics are the same as those in the other lamellar cuprate systems, with the energetics dominated by the strong in-plane exchange interaction. The xy anisotropy in these interactions, as determined from energy gap measurements in the spin-wave spectrum, is also the same order of magnitude as observed for the other lamellar CuO materials. The origin of the interaction which stabilizes the noncollinear spin structure still needs to be identified, and one possibility is an interlayer biquadratic exchange interaction. Whatever the origin, in our view the noncollinear struc-

ture is likely a universal property of the T' systems. This interaction should manifest itself as a gap in the spin-wave spectrum, and experimental techniques such as Raman scattering, magnetic resonance, or high-resolution neutron scattering should, in principle, be able to settle this question.

There are also some differences in the magnetic properties among the various members of the tetragonal R_2CuO_4 systems that warrant further investigation. One puzzle concerns the magnetic phase diagram, where measurements to lower temperatures in Pr_2CuO_4 would be desirable to ascertain whether the AF-$R_\perp$ phase boundary eventually turns over at low temperatures as found in Eu_2CuO_4 and Nd_2CuO_4.[32,44] In addition, the dependence of the rotation angle θ at low T for the Cu spin direction as a function of applied field along $[1\bar{1}0]$ also differs from Nd_2CuO_4 and Sm_2CuO_4. It will also be very interesting to make diffraction measurements for fields along [100], which is the zero-field spin direction.

ACKNOWLEDGMENTS

Research at the University of Maryland is supported by the NSF, DMR 93-02380. The NG-5 SPINS spectrometer is supported in part by NSF, DMR 91-22444.

[1]For a review, see J. W. Lynn, in *Physical and Material Properties of High Temperature Superconductors,* edited by S. K. Malik and S. S. Shah (Nova Science, New York, 1994), p. 243; see also *High Temperature Superconductivity,* edited by J. W. Lynn (Springer, New York, 1990).

[2]A. G. Gukasov, S. Y. Kokovin, V. P. Plakhty, I. A. Zobkalo, S. N. Barilo, and D. I. Zhigunov, Physica B **180**, 455 (1992); M. J. Rosseinsky, K. Prassides, and P. Day, J. Chem. Soc. Chem. Comm. **22**, 1734 (1989).

[3]S. Skanthakumar, H. Zhang, T. W. Clinton, I. W. Sumarlin, W.-H. Li, J. W. Lynn, Z. Fisk, and S.-W. Cheong, J. Appl. Phys. **64**, 4530 (1990); S. Skanthakumar, H. Zhang, T. W. Clinton, W-H. Li, J. W. Lynn, Z. Fisk, and S.-W. Cheong, Physica C **160**, 124 (1989).

[4]M. Matsuda, K. Yamada, K. Kakurai, H. Kadowaki, T. R. Thurston, Y. Endoh, Y. Hidaka, R. J. Birgeneau, M. A. Kastner, P. M. Gehring, A. H. Moudden, and G. Shirane, Phys. Rev. B **42**, 10098 (1990); M. Matsuda, Y. Endoh, K. Yamada, H. Kojima, I. Tanaka, R. J. Birgeneau, M. A. Kastner, and G. Shirane, *ibid.* **45**, 12548 (1992).

[5]S. Skanthakumar, J. W. Lynn, J. L. Peng, and Z. Y. Li, J. Magn. Magn. Mater. **104-107**, 519 (1992); T. Chattopadhyay, P. J. Brown, and U. Köbler, Physica C **177**, 294 (1991).

[6]D. E. Cox, A. I. Goldman, M. A. Subramanian, J. Gopalakrishnan, and A. W. Sleight, Phys. Rev. B **40**, 6998 (1989); P. Allenspach, S.-W. Cheong, A. Dommann, P. Fischer, Z. Fisk, A. Furrer, H. R. Ott, and B. Rupp, Z. Phys. B **77**, 185 (1989); S. Katano, R. M. Nicklow, S. Funahashi, N. Môri, T. Kobayashi, and J. Akimitsu, Physica C **215**, 92 (1993).

[7]T. Chattopadhyay, J. W. Lynn, N. Rosov, T. E. Grigereit, S. N. Barilo, and D. I. Zhigunov, Phys. Rev. B **49**, 9944 (1994).

[8]T. R. Thurston, M. Matsuda, K. Kakurai, K. Yamada, Y. Endoh, R. J. Birgeneau, P. M. Gehring, Y. Hidaka, M. A. Kastner, T. Murakami, and G. Shirane, Phys. Rev. Lett. **65**, 263 (1990).

[9]M. B. Maple, N. Y. Ayoub, T. Bjørnholm, E. A. Early, S. Ghamaty, B. W. Lee, J. T. Markert, J. J. Neumeier, and C. L. Seaman, Physica C **164**, 296 (1989).

[10]M. F. Hundley, J. D. Thompson, S.-W. Cheong, Z. Fisk, and S. B. Oseroff, Physica C **158**, 102 (1989); C. L. Seaman, N. Y. Ayoub, T. Bjørnhorm, E. A. Early, S. Ghamaty, B. W. Lee, J. T. Markert, J. J. Neumeier, P. K. Tsai, and M. B. Maple, *ibid.* **159**, 391 (1989).

[11]S. Ghamaty, B. W. Lee, J. T. Markert, E. A. Early, T. Bjørnholm, C. L. Seaman, and M. B. Maple, Physica C **160**, 217 (1989).

[12]I. W. Sumarlin, S. Skanthakumar, J. W. Lynn, J. L. Peng, Z. Y. Li, W. Jiang, and R. L. Greene, Phys. Rev. Lett. **68**, 2228 (1992); S. Skanthakumar, J. W. Lynn, J. L. Peng, and Z. Y. Li, J. Appl. Phys. **69**, 4866 (1991).

[13]J. W. Lynn, I. W. Sumarlin, S. Skanthakumar, W.-H. Li, R. N. Shelton, J. L. Peng, Z. Fisk, and S.-W. Cheong, Phys. Rev. B **41**, 2569 (1990).

[14]P. E. Sulewski, P. A. Fleury, K. B. Lyons, S.-W. Cheong, and Z. Fisk, Phys. Rev. B **41**, 225 (1990); S. Sugai, T. Kobayashi, and J. Akimitsu, *ibid.* **40**, 2686 (1989).

[15]For a theoretical review of the 2D $S=\frac{1}{2}$ Heisenberg antiferromagnet, see E. Manousakis, Rev. Mod. Phys. **63**, 1 (1991).

[16]S. Chakravarty, B. I. Halperin, and D. R. Nelson, Phys. Rev. Lett. **60**, 1057 (1988); Phys. Rev. B **39**, 2344 (1989).

[17]P. Hasenfratz and F. Niedermayer, Phys. Lett. B **268**, 231 (1991).

[18]M. Greven, R. J. Birgeneau, Y. Endoh, M. A. Kastner, B. Keimer, M. Matsuda, G. Shirane, and T. R. Thurston, Phys. Rev. Lett. **72**, 1096 (1994).

[19]I. W. Sumarlin, J. W. Lynn, D. A. Neumann, J. J. Rush, C.-K. Loong, J. L. Peng, and Z. Y. Li, Phys. Rev. B **48**, 473 (1993); J. W. Lynn, I. W. Sumarlin, D. A. Neumann, J. J. Rush, J. L. Peng, and Z. Y. Li, Phys. Rev. Lett. **66**, 919 (1991).

[20]C.-K. Loong and L. Soderholm, Phys. Rev. B **48**, 14001 (1993); J. Alloys Compounds **181**, 241 (1992).

[21]A. T. Boothroyd, S. M. Doyle, D. McK. Paul, and R. Osborn, Phys. Rev. B **45**, 10075 (1992).

[22]V. Nekvasil, Physica C **170**, 469 (1990).

[23]P. Allenspach, A. Furrer, R. Osborn, and A. D. Taylor, Z. Phys. B **85**, 301 (1991); P. Allenspach, S.-W. Cheong, A. Dommann, P. Fischer, Z. Fisk, A. Furrer, H. R. Ott, and B. Rupp, *ibid.* **77**, 185 (1989).

[24]I. W. Sumarlin, J. W. Lynn, T. Chattopadhyay, S. N. Barilo, and D. I. Zhigunov, Physica C **219**, 195 (1994).

[25]For a detailed discussion on magnetic properties of a singlet-ground-state system, see J. Jensen and A. R. Mackintosh, *Rare-Earth Magnetism Structures and Excitations* (Oxford University Press, New York, 1991); see also B. R. Cooper, in *Magnetic Properties of Rare Earth Metals,* edited by R. J. Elliott (Plenum, London, 1972), Chap. 2, and references therein.

[26]J. G. Houmann, M. Chapellier, A. R. Mackintosh, P. Bak, O. D. McMasters, and K. A. Gschneidner, Jr., Phys. Rev. Lett. **34**, 587 (1975).

[27]J. G. Houmann, B. D. Rainford, J. Jensen, and A. R. Mackintosh, Phys. Rev. B **20**, 1105 (1979); J. Jensen, J. Phys. (Paris)

Colloq. **5**, C5-1 (1979); P.-A. Lingård and J. G. Houmann, Proceedings of the Conference on Rare Earth and Actinides, Durham [Conf. Digest **3**, 192 (1971)].

[28]J. L. Peng, Z. Y. Li, and R. L. Greene, Physica C **177**, 79 (1991); J. L. Peng and R. L. Greene, *ibid.* **172**, 79 (1990).

[29]P. G. Radaelli, J. D. Jorgensen, A. J. Schultz, J. L. Peng, and R. L. Greene, Phys. Rev. B **49**, 15 322 (1994), and references therein.

[30]S. Skanthakumar, Ph.D thesis, University of Maryland, 1993.

[31]I. W. Sumarlin, Ph.D thesis, University of Maryland, 1994.

[32]S. Skanthakumar, J. W. Lynn, J. L. Peng, and Z. Y. Li, Phys. Rev. B **47**, 6173 (1993).

[33]S. Skanthakumar, J. W. Lynn, J. L. Peng, and Z. Y. Li, J. Appl. Phys. **73**, 6326 (1993); D. Petitgrand, A. H. Moudden, P. Galez, and P. Boutrouille, J. Less-Common Metals **164-165**, 768 (1990).

[34]D. A. Yablonsky, Physica C **182**, 105 (1991).

[35]V. A. Blinkin, I. M. Vitebskii, O. D. Kolotii, N. M. Lavrinenko, V. P. Seminozhenko, and V. L. Sobolev, Sov. Phys. JETP **71**, 1179 (1990).

[36]V. L. Sobolev, H. L. Huang, I. M. Vitebskii, A. N. Knigavko, and Y. G. Pashkevich, Phys. Rev. B **48**, 3417 (1993).

[37]T. Thio, T. R. Thurston, N. W. Preyer, P. J. Picone, M. A. Kastner, H. P. Jenssen, D. R. Gabbe, C. Y. Chen, R. J. Birgeneau, and A. Aharony, Phys. Rev. B **38**, 905 (1988); M. A. Kastner, R. J. Birgeneau, T. R. Thurston, P. J. Picone, H. P. Jenssen, D. R. Gabbe, M. Sato, K. Fukuda, S. Shamoto, Y. Endoh, K. Yamada, and G. Shirane, Phys. Rev. B **38**, 6636 (1988).

[38]B. Keimer, A. Aharony, A. Auerbach, R. J. Birgeneau, A. Cassanho, Y. Endoh, R. W. Erwin, M. A. Kastner, and G. Shirane, Phys. Rev. B **45**, 7430 (1992).

[39]T. Yildirium, A. B. Harris, O. Entin-Wohlman, and A. Aharony, Phys. Rev. Lett. **72**, 3710 (1994).

[40]S. Skanthakumar, J. W. Lynn, and I. W. Sumarlin (unpublished).

[41]D. A. Yablonsky and S. Skanthakumar (private communication).

[42]See, for example, J. W. Lynn, P. Heller, and N. A. Lurie, Phys. Rev. B **16**, 5032 (1977).

[43]T. Thio, C. Y. Chen, B. S. Freer, D. R. Gabbe, H. P. Jenssen, M. A. Kastner, P. J. Picone, N. W. Preyer, and R. J. Birgeneau, Phys. Rev. B **41**, 231 (1990).

[44]T. Grigereit (private communication).

[45]Y. Endoh, K. Yamada, R. J. Birgeneau, D. R. Gabbe, H. P. Jenssen, M. A. Kastner, C. J. Peters, P. J. Picone, T. R. Thurston, J. M. Tranquada, G. Shirane, Y. Hidaka, M. Oda, Y. Enomoto, M. Suzuki, and T. Murakami, Phys. Rev. B **37**, 7443 (1988); G. Shirane, Y. Endoh, R. J. Birgeneau, M. A. Kastner, Y. Hidaka, M. Oda, M. Suzuki, and T. Murakami, Phys. Rev. Lett. **59**, 1613 (1987).

[46]V. L. Sobolev, H. L. Huang, Y. G. Pashkevich, M. M. Larionov, I. M. Vitebsky, and V. A. Blinkin, Phys. Rev. B **40**, 1170 (1994).

[47]G. Aeppli, S. M. Hayden, H. A. Mook, Z. Fisk, S.-W. Cheong, D. Rytz, J. P. Remeika, G. P. Espinosa, and A. S. Cooper, Phys. Rev. Lett. **62**, 2052 (1989).

[48]S. M. Hayden, G. Aeppli, R. Osborn, A. D. Taylor, T. G. Perring, S.-W. Cheong, and Z. Fisk, Phys. Rev. Lett. **67**, 3622 (1991).

[49]P. Bourges, L. Boudarene, D. Petitgrand, and P. Galez, Physica B **180&181**, 447 (1992); P. Bourges, A. S. Ivanov, D. Petitgrand, J. Rossat-Mignod, and L. Boudarene, *ibid.* **186-188**, 925 (1993).

[50]V. V. Eremenko, S. A. Zvyagin, V. V. Pishko, V. V. Tsapenko, S. N. Barilo, and D. I. Zhigunov, JETP Lett. **52**, 338 (1990); A. I. Smirnov, S. N. Barilo, and D. I. Zhigunov, Sov. Phys. JETP **73**, 934 (1991).

[51]C. J. Peters, R. J. Birgeneau, M. A. Kastner, H. Yoshizawa, Y. Endoh, J. Tranquada, G. Shirane, Y. Hidaka, M. Oda, M. Suzuki, and T. Murakami, Phys. Rev. B **37**, 9761 (1988).

[52]I. M. Vitebskii, A. V. Yeremenko, Y. G. Pashkevich, V. L. Sobolev, and S. A. Fedorov, Physica C **178**, 189 (1991).

[53]J. Jensen, J. Phys. C **9**, 111 (1976).

[54]K. N. Clausen, K. A. McEwen, J. Jensen, and A. R. Mackintosh, Phys. Rev. Lett. **72**, 3104 (1994).

[55]B. R. Cooper, Phys. Rev. B **6**, 2730 (1972).

[56]R. J Birgeneau, J. Als-Nielsen, and E. Bucher, Phys. Rev. B **6**, 2724 (1972).

[57]E. Bucher, J. P. Maita, and A. S. Cooper, Phys. Rev. B **6**, 2709 (1972); K. Andres, E. Bucher, S. Darack, and J. P. Maita, *ibid.* **6**, 2716 (1972).

[58]A. S. Ivanov, N. L. Mitrofanov, A. Y. Rumyantsev, L. Pintschovius, N. Pyuka, and W. Reichardt, Sov. J. Low Temp. Phys. **17**, 693 (1991); L. Pintschovius, N. Pyka, W. Reichardt, A. Y. Rumiantsev, N. L. Mitrofanov, A. S. Ivanov, G. Collin, and P. Bourges, Physica C **185-189**, 156 (1991).

[59]J. A. Sanjuro, C. Rettori, S. Oseroff, and Z. Fisk, Phys. Rev. B **49**, 4391 (1994).

[60]P-A. Lingård, J. Phys. C **8**, L179 (1975).

[61]J. Jensen, J. Phys. C **15**, 2403 (1982).